

# Collisional broadening, shifting, narrowing, and mixing of H<sub>2</sub>O doublet lines nearby 5 $\mu\text{m}$

A. Valentin\*, Ch. Claveau\*, V.P. Kochanov, and V.N. Saveliev

*Institute of Atmospheric Optics,  
Siberian Branch of the Russian Academy of Sciences, Tomsk, Russia  
\*Laboratory of Molecular Physics and Applications,  
Pierre and Mary Curie VI University, Paris, France*

Received June 21, 1999

The line profiles for seven H<sub>2</sub>O absorption doublet lines nearby 2000  $\text{cm}^{-1}$  have been measured with the Fourier transform spectrometer of Paris VI University at different pressures of the buffer gas (nitrogen and argon). The data were processed on the basis of numerical solution of the convolution equation corresponding to the recorded spectra and theoretical line profiles describing both the collisional narrowing and mixing of lines. The absolute line intensities, pressure broadening and shift coefficients, as well as the parameters of narrowing and mixing were determined. It was found that the effect of line mixing on the profiles of resolved and unresolved doublets is negligible, while the narrowing significantly affects some doublets.

## Introduction

A large signal-to-noise ratio (about 100) and high resolution (about 0.005  $\text{cm}^{-1}$ ) that are typical of Fourier transform spectrometers allow the numerical study of a line profile. Thus, absolute intensities and pressure broadening and shift coefficients can be reliably determined for homogeneously broadened lines. However, when studying finer collisional processes, such as line narrowing<sup>1-3</sup> and mixing,<sup>4-7</sup> with use of the Fourier transform spectroscopy, the instrumental function of a spectrometer should be adequately taken into account, because its width is comparable with the Doppler width of IR absorption lines, and the indicated processes manifest themselves mostly in the area of inhomogeneous broadening.

Unresolved and overlapping H<sub>2</sub>O absorption doublet lines and the lines of other symmetric molecules possessing the hyperfine (cluster) structure of energy levels are of greatest interest from the viewpoint of studying the collisional narrowing and mixing (spectral exchange, cross-relaxation).<sup>8</sup> The point is that such doublets result from clusterization of energy levels which occurs at large values of rotational moments. According to the physics of collisional line broadening,<sup>9,10</sup> the broadening constants under such conditions are small, and thus the line narrowing is more pronounced. Simultaneously, mixing of multiplet lines must show itself, especially, in the case of the line overlapping until complete merging (collapse) with growing pressure. In particular, in Ref. 11 it was shown with the aid of laser spectroscopy technique that for the  $\nu_3$  band of the CH<sub>4</sub> molecule the spectral exchange among overlapping lines gives a detectable contribution to their common profile.

At the same time, the numerical processing of such doublets in the Fourier transform spectroscopy was

hampered until recently by the absence of a reliable technique for elimination of the effect of the spectrometer instrumental function on the line shape at low pressure of the buffer gas, as well as by the absence of theoretical models of the line profile which simultaneously take into account both narrowing and mixing of spectral lines as a result of inelastic collisions changing the velocity of the molecule and inducing the spectral exchange.<sup>12,13</sup>

This paper is devoted to processing of the experimental data on the doublet line profiles of the  $\nu_2$  band of H<sub>2</sub>O in the range from 1848.8 to 2161.7  $\text{cm}^{-1}$ . The data were recorded with the Fourier transform spectrometer at the Paris VI University at the buffer gas pressure (nitrogen and argon) from 40 to 800 Torr and at the absolute temperature from 296 to 299 K. The absolute intensities and the broadening and shift coefficients were determined for the seven doublet lines, two of which were fully resolved at low pressure. The technique to eliminate the distorting effect of the spectrometer instrumental function on the line shape has been developed, as well as the model of a spectral line profile allowing for both the line narrowing and mixing effects.<sup>12,13</sup> Application of this model to processing of the experimental line profiles has allowed us to evaluate the degree of these effects influence on the shape of resolved and unresolved doublets and to find the values of parameters of the narrowing and spectral exchange.

## The method for eliminating the effect of the instrumental function of the Fourier transform spectrometer on the recorded spectra

It is known from the theory of Fourier transform spectroscopy<sup>14</sup> that in the case of small optical depth

the instrumental function of FT spectrometers  $f_{\text{inst}}(\nu)$  is related with the shape of the recorded spectrum  $f_{\text{exp}}(\nu)$  as:

$$\int_{-\infty}^{\infty} f_{\text{inst}}(\nu - x) f(x) dx = f_{\text{exp}}(\nu), \quad (1)$$

where the sought function  $f(\nu)$  is the true spectrum, not distorted by the instrumental function (the profile of an isolated line or several spectral lines).

The technique for solution of the ill-posed problem for Fredholm equations of the second kind (in this case the convolution equation) with the right-hand side distorted by noise and the known function  $f_{\text{inst}}(\nu)$  is well developed.<sup>15,16</sup> This technique is based on the method for numerical solution of Eq. (1) with use of the discrete Fourier transform followed by Tikhonov regularization of the solution.<sup>16</sup>

To find the unknown instrumental function, we will use the experimental records of absorption line profiles of a molecule different from the molecule under study. The absorption spectra of such molecules are recorded in a separate cell inside a spectrometer at low gas pressure simultaneously with the spectrum under study, and they serve as a reference. In our measurements, the CO gas at the pressure less than 0.1 Torr was used as a reference. The profiles of the CO isolated lines are not distorted by the instrumental function, so they are Doppler profiles to high accuracy, and their width and shape are well-known. Thus, the equation for the instrumental function is the following:

$$\int_{-\infty}^{\infty} f_{\text{inst}}(\nu - x) f_{\text{D}}(x) dx = f_{\text{D}}^{\text{exp}}(\nu); \quad (2)$$

$$f_{\text{D}}(\nu) = \frac{S_{\text{r}}}{\sqrt{\pi} k \bar{\nu}} \exp[-(\nu/k\bar{\nu})^2], \quad \bar{\nu} = \sqrt{2k_{\text{B}}T/m}.$$

Here  $f_{\text{D}}(\nu)$  is the initial Doppler profile of a line of the reference molecule;  $f_{\text{D}}^{\text{exp}}(\nu)$  is the recorded profile;  $S_{\text{r}}$  is the absolute intensity;  $k$  is the wave number of the given line;  $k_{\text{B}}$  is the Boltzmann constant;  $m$  is the mass of the reference molecule;  $T$  is the gas temperature;  $\bar{\nu}$  is the mean thermal speed of the absorbing molecule.

Note that to find  $f_{\text{inst}}(\nu)$  from Eq. (2), it is desirable to use the heaviest molecules as the reference ones, the Doppler line widths of which are less than the width of the instrumental function to be estimated.

By applying the Fourier transforms to the functions entering into Eqs. (1) and (2), we obtain

$$F_{\text{inst}}(\sigma) = F_{\text{D}}^{\text{exp}}(\sigma) / F_{\text{D}}(\sigma); \quad (3)$$

$$F(\sigma) = F_{\text{exp}}(\sigma) / F_{\text{inst}}(\sigma) = F_{\text{exp}}(\sigma) F_{\text{D}}(\sigma) / F_{\text{D}}^{\text{exp}}(\sigma), \quad (4)$$

where the capital letters denote the Fourier transforms of the corresponding functions.

In accordance with the idea of the Tikhonov

regularization method, the regularization parameter  $\alpha$  should be introduced in the denominators of Eqs. (3) and (4). We also introduce the apodizing factor  $F_{\text{cut}}(\sigma)$ , which decreases the effect of noise in far wings of spectral lines. The problems of selection of the regularization parameter are discussed in the specialized literature (see, for example, Refs. 16 and 17). However, the case at hand is somewhat simpler, because the functions  $f_{\text{D}}(\nu)$  and  $f_{\text{D}}^{\text{exp}}(\nu)$  have a symmetric bell-shaped form. Therefore, the Fourier transforms  $F_{\text{D}}(\sigma)$  and  $F_{\text{D}}^{\text{exp}}(\sigma)$  are real, always positive, and have the same shape. In particular, the Fourier transform  $F_{\text{D}}(\sigma)$  can be calculated analytically:

$$F_{\text{D}}(\sigma) = \int_{-\infty}^{\infty} f_{\text{D}}(\nu) \exp[-2\pi i \sigma \nu] d\nu = S_{\text{r}} \exp[-(\pi k \bar{\nu} \sigma)^2]. \quad (5)$$

As the numerical calculations show, the initial spectrum  $f_{\text{D}}(\nu)$  can be reconstructed with maximum relative error at the line center below 0.3% by selecting  $\alpha = 0$  near the center  $F_{\text{D}}(\sigma = 0)$  and gradually increasing with the distance away from the center up to the constant value  $\alpha = \alpha_0$  at the level (0.01 – 0.001)  $F_{\text{D}}(0)$ .

Thus, in spite of Eqs. (3) and (4) we have

$$F_{\text{inst}}(\sigma) = F_{\text{cut}}(\sigma) F_{\text{D}}^{\text{exp}}(\sigma) / (F_{\text{D}}(\sigma) + \alpha(\sigma)); \quad (6)$$

$$F(\sigma) = F_{\text{cut}}(\sigma) F_{\text{exp}}(\sigma) / F_{\text{inst}}(\sigma) = F_{\text{cut}}(\sigma) F_{\text{exp}}(\sigma) F_{\text{D}}(\sigma) / (F_{\text{D}}^{\text{exp}}(\sigma) + \alpha(\sigma)); \quad (7)$$

$$\alpha(\sigma) = \alpha_0 \{1 - \exp[-(\sigma/b)^{10}]\};$$

$$F_{\text{cut}}(\sigma) = \exp[-(\sigma/c)^{10}].$$

The discrete numerical Fourier transform applied to Eqs. (6) and (7) gives the sought spectrum  $f(\nu)$  free of the instrumental function effect, as well as the instrumental function itself  $f_{\text{inst}}(\nu)$ . The parameters  $b$ ,  $c$ , and  $\alpha_0$  are selected based on the widths and amplitudes of the functions  $F_{\text{D}}(\sigma)$  and  $F_{\text{D}}^{\text{exp}}(\sigma)$ . In the processing procedure the shape of  $f_{\text{D}}^{\text{exp}}(\nu)$  was averaged over 10 to 12 cases corresponding to several lines, upon reducing the maximum amplitude of the profiles to the unit one and normalizing the frequency to the halfwidths  $k\bar{\nu}$  of the Doppler profiles at the height  $1/e$ . Then the area of  $f_{\text{D}}^{\text{exp}}(\nu)$  was normalized to unity, and it was assumed that  $S_{\text{r}} = 1$ . The calculations have shown that the shape of the instrumental function and the reconstructed spectra of H<sub>2</sub>O within several hundreds of cm<sup>-1</sup> are practically independent of the spectral position of qn lines, over which the results were averaged. So, in the further processing the instrumental function was assumed to be frequency independent. The shape of  $f_{\text{inst}}(\nu)$  for different values of  $\alpha_0$  belonging to the class of solutions of Eqs. (1) and (2) is shown in Fig. 1.

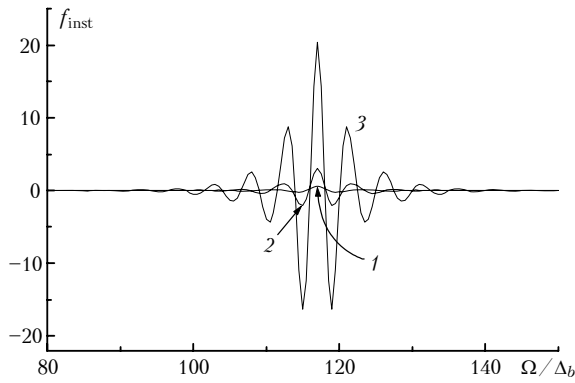


**Fig. 1.** The shape of the instrumental function of the FT spectrometer at different values of the regularization parameter  $\alpha_0 = 10^{-2}$  (curve 1),  $10^{-3}$  (2),  $10^{-4}$  (3).

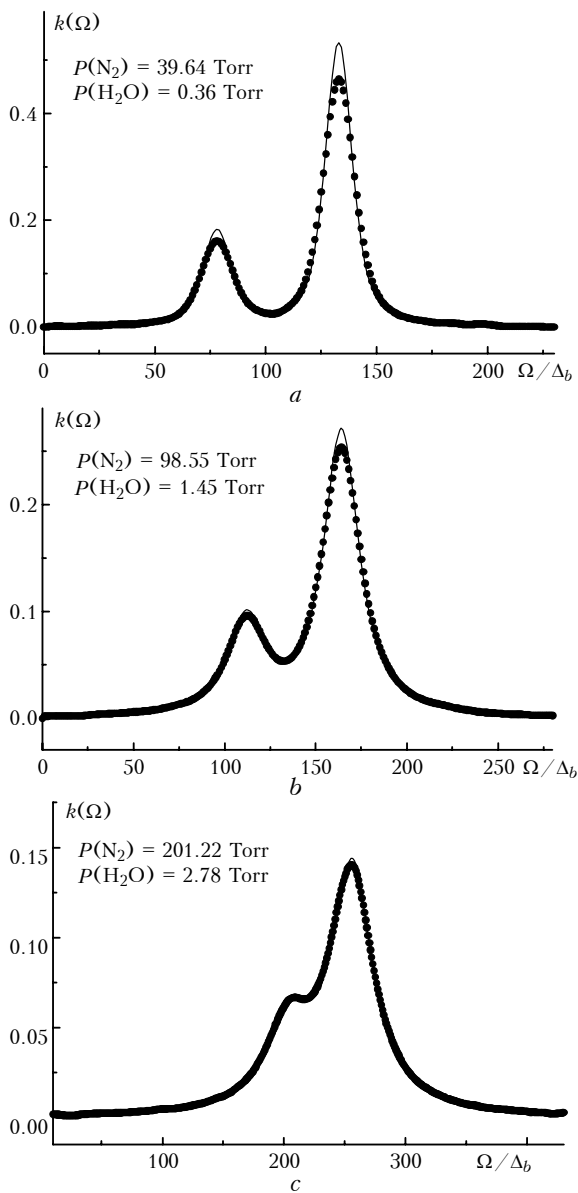


**Fig. 2.** Profile of the line at  $2115 \text{ cm}^{-1}$  (solid curve) reconstructed from the experimental profile (dots) at different pressure of water vapor and buffer gas (nitrogen).

The profiles  $f(\nu)$  reconstructed with the indicated values of  $\alpha_0$  are indistinguishable. The examples of reconstruction of the profiles of a resolved doublet with the center  $\nu_0 = 2115 \text{ cm}^{-1}$  recorded at different pressures of nitrogen and water vapor are shown in Fig. 2.

## Processing procedure and experimental results

The spectrometer and experimental conditions are described in Ref. 18. The measurements were conducted at two base optical pathlengths, and the corresponding steps of the discrete frequency tuning were  $\Delta_b = 6.3436 \cdot 10^{-4}$  and  $6.0265 \cdot 10^{-4} \text{ cm}^{-1}$ . The primary processing of individual doublet lines was in determination of the level of zero absorption. The approximation model consisted of the sum of one or, for two doublets, two Voigt profiles and a small wavy pedestal approximated by the sine and a constant term. This model was fitted to the experimental profiles using the least-square method. The examples of the primary processing can be found in Ref. 19. The next step was elimination of the instrumental function influence. It was done in accordance with the technique considered in the previous section. The instrumental function was determined for each of the two above values of  $\Delta_b$ . The last stage of the processing involved the least-square fitting of two theoretical models to the experimental profiles. The fitted models were the following: the profile  $k_{\text{nar}}(\omega)$  derived within the hard collision model<sup>3,20,21</sup> and taking into account the collisional narrowing; the profile  $k_{\text{mix}}(\omega)$  derived within the same model<sup>12,13</sup> and taking into account the mixing of doublet components along with the collisional narrowing. The corresponding equations are:

$$k_{\text{nar}}(\omega) = \frac{1}{\pi \tilde{\nu}} \text{Re} \left[ \frac{S_1 \omega_1}{1 - \omega_1} + \frac{S_2 \omega_2}{1 - \omega_2} \right]; \quad (8)$$

$$\omega_n \equiv \sqrt{\pi} \frac{\tilde{\nu}}{k \bar{\nu}} \omega \left( \frac{\omega - \nu_{0n} + i\nu}{k \bar{\nu}} \right),$$

$$\omega(z) = \frac{i}{\pi} \int_{-\infty}^{\infty} \frac{e^{-t^2} dt}{z - t}, \quad n = 1, 2;$$

$$k_{\text{nar}}(\omega) = \frac{1}{\pi} \times$$

$$\times \text{Re} \left[ \frac{S_1 u_1 + S_2 u_2 - [\tilde{\nu}(S_1 + S_2) - (\sqrt{3} + 1/\sqrt{3}) \zeta \sqrt{S_1 S_2}] u_1 u_2}{1 - \tilde{\nu}(u_1 + u_2) + (\tilde{\nu}^2 - \zeta^2) u_1 u_2} \right]; \quad (9)$$

$$u_n \equiv \frac{\sqrt{\pi}}{k \bar{\nu}} \omega \left( \frac{\omega - \nu_{0n} + i\nu}{k \bar{\nu}} \right), \quad n = 1, 2.$$

Here  $\omega$  is the frequency;  $S_1$  and  $S_2$  are the intensities of the doublet components;  $\nu_{01}$  and  $\nu_{02}$  are their spectral positions;  $\nu$  is the output frequency of the collision

integral;  $\tilde{\nu}$  and  $\zeta$  are the input frequencies of the collision integral due to elastic and inelastic collisions<sup>22,23</sup> (the latter is also known as a cross-relaxation parameter);  $\omega(z)$  is the complex probability function.

Further it is convenient to use the dimensionless and buffer-gas-pressure independent parameters of narrowing  $\alpha$  and spectral exchange  $\xi$ :

$$\alpha \equiv \tilde{\nu}/\gamma, \quad \xi \equiv \zeta/\gamma, \quad \gamma = \nu - \tilde{\nu}, \quad (10)$$

where  $\gamma$  is the homogeneous (collisional) line halfwidth at high gas pressure without line mixing.

In Eqs. (8) and (9) the input and output frequencies are considered real and equal for the both doublet components. This decreases the number of fitting parameters and, as resulted from the processing, well corresponds to the experiment. It was assumed in the processing of the unresolved doublets in accordance with the symmetry of the  $m_2n$  molecule that  $S_2/S_1 = 3$  (or  $1/3$ ), and the separation between the doublet components was fixed and taken equal to the calculated value known from the literature. The processing in that case gave the total intensity of the doublet line. Such a processing method can be reasoned by the following circumstance. As the processing results have shown, for two resolved doublets at  $\nu_0 = 2115$  and  $2041 \text{ cm}^{-1}$  the separation between the centers of their components was practically pressure-independent.

The least-square fitting of Eqs. (8) and (9) for each realization of the profiles at a certain pressure gave the values of the fitting parameters  $S_1$  and  $S_2$  ( $S = S_1 + S_2$ ),  $\nu_{01}$  and  $\nu_{02}$ ,  $\gamma$ ,  $\alpha$ , and  $\xi$ . The typical result of the fitting is shown in Fig. 3. The average values of line intensities normalized to the water vapor pressure and corresponding to different pressures of the buffer gas were used to correct the pressure of water vapor measured with inadequate reliability. The relative corrections did not exceed 10% and were on average 5%. The spread of the determined intensities is illustrated in Fig. 4. The average measured values of

the absolute intensities are tabulated in Table 1 in comparison with the measured results<sup>24</sup> and theoretical calculations.<sup>25</sup> The assignment and positions of the spectral lines are borrowed from Ref. 25.

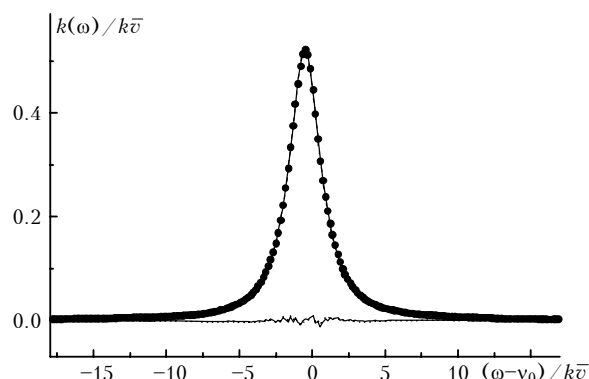


**Fig. 3.** Experimental profile of the line at  $2136.14 \text{ cm}^{-1}$  free from the influence of the instrumental function at the water vapor pressure of 1.5 Torr and nitrogen pressure of 98.5 Torr (dots) and the theoretical profiles (8) and (9) fitted to it (indistinguishable solid curves). The lower curves are the difference between the experiment and model (8) (solid curve) and the difference between the experiment and model (9) (dots).

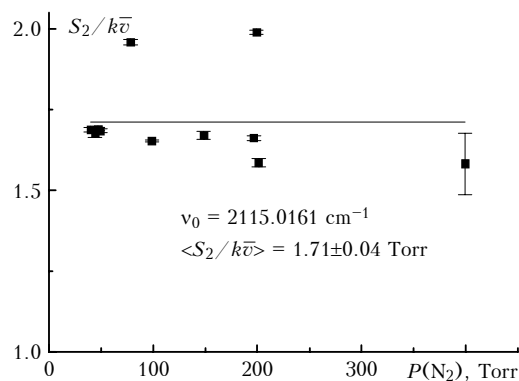


**Fig. 4.** Absolute intensities (normalized to the water vapor pressure) of the most intense component of the doublet line at  $2115 \text{ cm}^{-1}$  at different pressures of water vapor and the buffer gas.

**Table 1**

$\nu_0, \text{ cm}^{-1}$	$J \ K_a \ K_c$ upper level	$J \ K_a \ K_c$ lower level	$10^3 S,$ $\text{cm}^{-2}\cdot\text{atm}^{-1}$	$\delta S/S,$ %	$10^3 S$ (Ref. 24), $\text{cm}^{-2}\cdot\text{atm}^{-1}$	$\delta S/S,$ %	$10^3 S$ (Ref. 25), $\text{cm}^{-2}\cdot\text{atm}^{-1}$	$S_2/S_1$ ( $S_1/S_2$ )	$\frac{\delta(S_2/S_1)}{S_2/S_1},$ %
1848.8114	14 0 14	13 1 13	3.91	12.6	4.30	6	4.04	2.76	15.0
1848.8152	14 1 14	13 0 13	10.78	2.4	12.9	6	12.11		
1864.0561	15 0 15	14 1 14	5.05	5.1	5.30	6	4.87	-	-
1864.0580	15 1 15	14 0 14							
1879.0188	16 0 16	15 1 15	1.41	3.0	1.29	3	1.34	-	-
1879.0197	16 1 16	15 0 15							
2041.2884	8 6 3	7 5 2	41.31	2.9	39.1	3	38.83	2.90	2.5
2041.4957	8 6 2	7 5 3	14.28	8.9	13.7	3	12.93		
2114.9831	9 7 3	8 6 2	2.17	8.4	2.09	3	2.01	2.93	6.3
2115.0161	9 7 2	8 6 3	6.35	0.8	6.25	3	6.02		
2136.1437	8 8 1	7 7 0	8.27	4.4	8.44	5	7.57	-	-
2136.1438	8 8 0	7 7 1							
2161.7256	9 8 2	8 7 1	3.11	2.8	2.85	4	2.80	-	-
2161.7263	9 8 1	8 7 2							

For the lines at 1879 and 2115 cm<sup>-1</sup> the water vapor pressure varied from 0.4 to 6 Torr. Thus, the pressure broadening and shift coefficients of that gas were estimated using the least-square method. The values obtained are the following:  $\gamma_0(\text{H}_2\text{O} - \text{H}_2\text{O}) = 0.27 \pm 0.45 \text{ cm}^{-1}\cdot\text{atm}^{-1}$  (2115 cm<sup>-1</sup>);  $0.12 \pm 0.08 \text{ cm}^{-1}\cdot\text{atm}^{-1}$  (1879 cm<sup>-1</sup>) and  $\Delta_0 = - (0.39 \pm 0.33) \text{ cm}^{-1}\cdot\text{atm}^{-1}$  (2115 cm<sup>-1</sup>);  $-(0.15 \pm 0.14) \text{ cm}^{-1}\cdot\text{atm}^{-1}$  (1879 cm<sup>-1</sup>). These values were used to construct the dependence of the lines collisional widths and shifts on the buffer gas (nitrogen and argon) pressure after subtraction of corrections for water vapor effect. As an example, Figs. 5 and 6 show the nitrogen pressure dependence of the collisional halfwidth and shift for the line at 2115 cm<sup>-1</sup>. The halfwidths  $\gamma$  used to construct the dependence shown in Fig. 5 were obtained from the profile (8) fitting accounting for the collisional narrowing of the line.

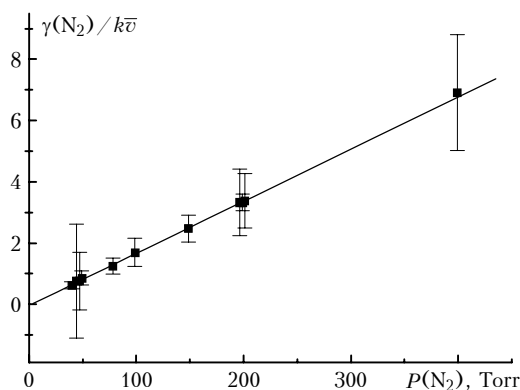


Fig. 5. Collisional halfwidths of the line at 2115 cm<sup>-1</sup> minus the part due to self-broadening vs. the nitrogen pressure.

Figure 7 illustrates the absence of the doublet components relative shift at varying nitrogen pressure. For other doublets the water vapor pressure varied in more narrow range (from 0.7 to 2.8 Torr), and the measurements were conducted at only four values of the buffer gas pressure (from 50 to 783 Torr). Therefore,

the results were not corrected for self-broadening and shift due to water vapor. The measured coefficients of broadening and shift for all doublets are presented in Table 2. The upper values in the table's rows were obtained from the processing by the model (8), whereas the lower values correspond to the model (9).

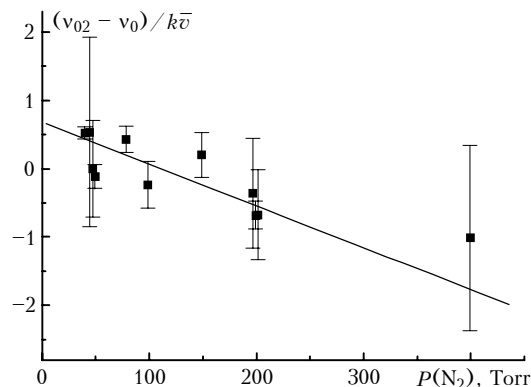


Fig. 6. Collisional shifts of the most intense component of the doublet at 2115 cm<sup>-1</sup> minus the shifts due to the water vapor pressure vs. the nitrogen pressure.

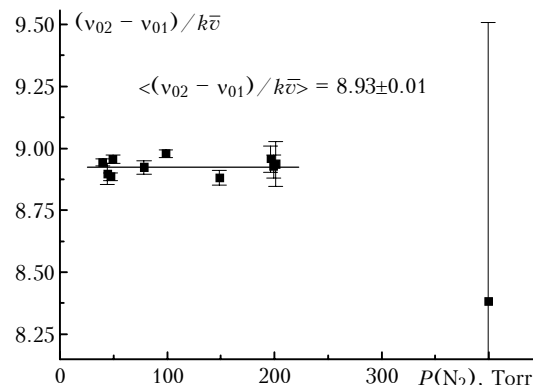


Fig. 7. Separation between the components of the doublet at 2115 cm<sup>-1</sup> vs. the nitrogen pressure.

Table 2

$\nu_0, \text{cm}^{-1}$	Buffer gas N <sub>2</sub>				Buffer gas Ar			
	$10^3 \gamma_0, \text{cm}^{-1}\cdot\text{atm}^{-1}$	$\delta\gamma/\gamma, \%$	$10^3 \Delta_0, \text{cm}^{-1}\cdot\text{atm}^{-1}$	$\delta\Delta_0/\Delta_0, \%$	$10^3 \gamma_0, \text{cm}^{-1}\cdot\text{atm}^{-1}$	$\delta\gamma/\gamma, \%$	$10^3 \Delta_0, \text{cm}^{-1}\cdot\text{atm}^{-1}$	$\delta\Delta_0/\Delta_0, \%$
1848.81	16.12	2.0	- 6.3	44	-	-	-	-
1848.82	15.42	5.7						
1864.06	9.75	7.6	- 2.0	116	3.75	3.4	- 5.03	0.4
	10.57	10.5			3.50	4.0		
1879.02	6.73	10.9	- 4.8	29	3.92	9.0	- 4.8	10
	6.73	8.3			2.78	21.6		
2041.29	61.3	0.6	- 12.3	3.3	-	-	-	-
2041.50	65.5	5.0						
2114.98	47.9	1.1	- 17	24	12.0	1.1	- 6.18	2.6
2115.02	47.8	1.2			12.2	2.0		
2136.14	28.6	0.7	- 9.56	6.5	-	-	-	-
	29.0	3.9						
2161.73	38.5	2.2	- 17	14	-	-	-	-
	39.6	1.6						

Table 3

$\nu_0, \text{cm}^{-1}$	Buffer gas $\text{N}_2$				Buffer gas Ar			
	$\langle\alpha\rangle$	$\delta\alpha/\alpha, \%$	$\langle\xi\rangle$	$\delta\xi/\xi, \%$	$\langle\alpha\rangle$	$\delta\alpha/\alpha, \%$	$\langle\xi\rangle$	$\delta\xi/\xi, \%$
1848.81	2.8	39	0.23	64	–	–	–	–
1848.82	5.7	38						
1864.06	1.5	51	0.16	45	2.77	7.1	0.5	38
	1.3	69			2.2	18		
1879.02	0.3	40	0.11	80	0.6	50	$2 \cdot 10^{-5}$	50
	0.2	56			0.6	50		
2041.29	7.8	24	0.04	81	–	–	–	–
2041.50	7.1	17						
2114.98	0.57	19	0.06	78	3.7	49	0.02	93
2115.02	0.60	20			3.6	46		
2136.14	1.13	32	1.1	100	–	–	–	–
	0.91	16						
2161.73	0.7	42	$4 \cdot 10^{-5}$	75	–	–	–	–
	0.7	42						

The averaged parameters  $\alpha$  and  $\xi$  determining, respectively, the degree of line narrowing and mixing are given in Table 3. Similarly to Table 2, the upper values in rows correspond to Eq. (8), while the lower ones correspond to Eq. (9). Figures 8 and 9 illustrate the spread in these parameters obtained from the processing of the profiles at different pressures. In these figures (as well as in the previous ones) the errors are indicated by the 95-% confidence intervals, which are about twice as large as the standard deviation. It follows from Table 3 that the widely separated lines of the doublets at 2041.29 and 2041.50  $\text{cm}^{-1}$  experience the strongest narrowing and line broadening due to argon is stronger than that due to nitrogen. The marked mixing of the doublet components is observed for only one recorded line at 2136.14  $\text{cm}^{-1}$ . The separation between components of this line is the smallest, and, according to the theory, is only  $10^{-4} \text{cm}^{-1}$ . The 95-% confidence interval for the cross-relaxation parameter related to the collisional line halfwidth is about  $3/4$  of the measured value of  $\xi$  which is, on average, much less than unity. So we can say that the influence of the spectral exchange between components of both resolved and unresolved doublet lines of  $m_2n$  nearby  $5 \mu\text{m}$  on their shape is insignificant. In contrast to mixing, the collisional narrowing for some doublets is significantly more pronounced. As the numerical calculations by Eq. (8) show, the total width of the line profile including both homogeneous and inhomogeneous components becomes markedly less than the Doppler width at  $\alpha > 2$ , and the observed values of  $\alpha$  are larger than these values for the nitrogen-broadened doublets at 1848.8 and 2041  $\text{cm}^{-1}$  and the argon-broadened doublets at 1864.1 and 2115  $\text{cm}^{-1}$ . It was found in the laser spectroscopy measurements<sup>26</sup> of the argon and xenon narrowing, that the line profile at 1879.02  $\text{cm}^{-1}$  is narrowed by 1.5 times as compared to the Doppler

profile. However, in our measurements the narrowing of this unresolved doublet is practically absent.

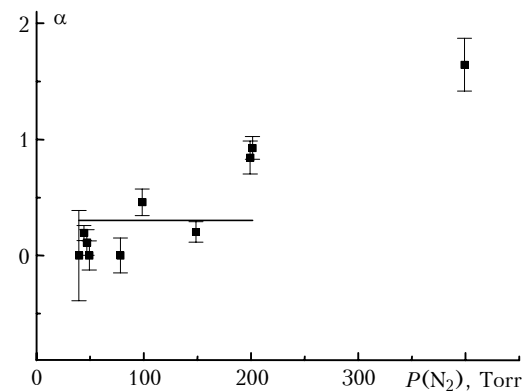


Fig. 8. The narrowing parameter derived from processing of the 1879- $\text{cm}^{-1}$  line profiles with the model (8) vs. the nitrogen pressure. The straight horizontal line corresponds to the average value of  $\alpha$ .

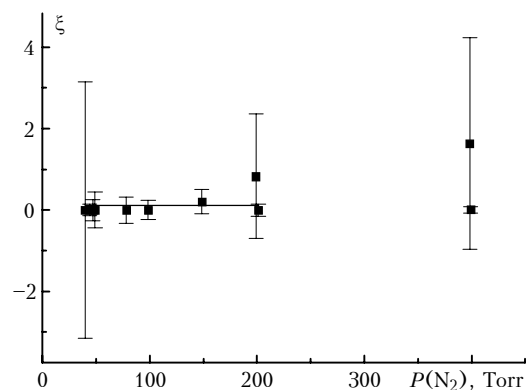


Fig. 9. The ratio of the cross-relaxation parameter  $\xi$  to the collisional halfwidth  $\gamma$  for the line at 1879  $\text{cm}^{-1}$  as a function of the buffer gas pressure. The straight horizontal line corresponds to the average value of  $\xi$ .

### Acknowledgments

V.P. Kochanov and V.N. Saveliev are indebted to A.D. Bykov and L.N. Sinita for useful discussions.

This work was partially supported by the Russian Foundation for Basic Research, Grant No. 98-02-17772.

### References

1. R.H. Dicke, Phys. Rev. **89**, No. 2, 472-473 (1953).
2. L. Galatry, Phys. Rev. **122**, No. 4, 1218-1223 (1961).
3. S.G. Rautian and I.I. Sobel'man, Usp. Fiz. Nauk **90**, No. 2, 209-236 (1966).
4. M. Baranger, Phys. Rev. **111**, No. 12, 492-504 (1958).
5. A.C. Kolb and H. Grim, Phys. Rev. **111**, No. 2, 514-521 (1958).
6. V. Fano, Phys. Rev. **131**, No. 1, 259-268 (1963).
7. A.I. Burshtein, *Lectures on Quantum Kinetics* (Novosibirsk State University Publishing House, Novosibirsk, 1968), 265 pp.
8. B.I. Zhilinskii, V.I. Perevalov, and V.I.G. Tyuterev, *Method of Irreducible Tensor Operators and the Theory of Molecular Spectra* (Nauka, Novosibirsk, 1987), 233 pp.
9. P.V. Anderson, Phys. Rev. **76**, No. 5, 647-661 (1949).
10. C.J. Tsao and B. Curnutte, J. Quant. Spectrosc. Radiat. Transfer **2**, No. 1, 41-91 (1962).
11. A.S. Pine, J. Quant. Spectrosc. Radiat. Transfer **57**, No. 2, 157-176 (1997).
12. Ch. Claveau, A. Valentin, V.P. Kochanov, V.N. Saveliev, and L.N. Sinita, Proc. SPIE **3583**, 106-112 (1998).
13. V.P. Kochanov, Atmos. Oceanic Opt. **12**, No. 9, 806-809 (1999).
14. G.N. Zhizhin, ed., *High-Resolution Infrared Spectroscopy* (Mir, Moscow, 1972), 352 pp.
15. A.N. Tikhonov and V.Ya. Arsenin, *Methods for Solution of Ill-Posed Problems* (Nauka, Moscow, 1986), 287 pp.
16. Yu.E. Voskoboinikov, N.G. Preobrazhenskii, and A.I. Sedel'nikov, *Mathematical Processing of the Experiment in Molecular Gas Dynamics* (Nauka, Novosibirsk, 1984), 239 pp.
17. Yu.E. Voskoboinikov and Ya.Ya. Tomson, Avtometriya, No. 4, 10-18 (1975).
18. A. Valentin, F. Rachet, A.D. Bykov, N.N. Lavrentieva, V.N. Saveliev, and L.N. Sinita, J. Quant. Spectrosc. Radiat. Transfer **59**, Nos. 3-5, 165-170 (1998).
19. A. Valentin, Ch. Claveau, A.D. Bykov, N.N. Lavrentieva, V.N. Saveliev, and L.N. Sinita, Proc. SPIE **3583**, 100-105 (1998).
20. M. Nelkin and A. Ghatak, Phys. Rev. **135**, No. 1A, A4-A9 (1964).
21. S.G. Rautian, Tr. Fiz. Inst. Akad. Nauk SSSR **43**, 3-115 (1968).
22. S.G. Rautian, G.I. Smirnov, and A.M. Shalagin, *Nonlinear Resonances in Atomic and Molecular Spectra* (Nauka, Novosibirsk, 1979), 312 pp.
23. S.G. Rautian and A.M. Shalagin, *Kinetic Problems of Non-linear Spectroscopy* (North-Holland, Amsterdam, 1991), 439 pp.
24. R.A. Toth, J. Opt. Soc. Am. **B8**, 2236-2255 (1991).
25. L.H. Coudert, J. Mol. Spectrosc. **181**, 246-273 (1997).
26. R.S. Eng, A.R. Calawa, T.C. Harman, P.L. Kelley, and A. Javan, Appl. Phys. Lett. **21**, No. 7, 303-305 (1972).